Resonance Auger decay after selective excitation of Kr 3*d* states by synchrotron radiation

H. Aksela, S. Aksela, and H. Pulkkinen
Department of Physics, University of Oulu, SF-90570 Oulu 57, Finland

G. M. Bancroft and K. H. Tan
Department of Chemistry and Centre for Chemical Physics, University of Western Ontario, London, Ontario, Canada N6A 5B7 and Canadian Synchrotron Radiation Facility, Synchrotron Radiation Center, University of Wisconsin, Stoughton, Wisconsin 53589
(Received 21 January 1986)

The $M_{4,5}NN$ normal and resonance Auger spectra of Kr have been measured using different photon energies to ionize or excite the 3*d* levels. Excitation of the 3*d* electrons to the $3d^9 4s^2 4p^6 5p$ resonance states results in decay with a 5*p* spectator or participator electron. The spectra are analyzed by comparing them with the calculated profiles. The calculations take into account the presence of a spectator electron, and the correlation effects in the case of a 4*s* hole state.

I. INTRODUCTION

Decay of the resonantly excited states of Kr and Xe has been of great interest in recent experimental studies using synchrotron radiation.[1–4] The spectra show a complicated fine structure. Besides the resonance Auger transitions with the excited electron as a spectator, autoionization lines are also present in which the excited electron takes part in the decay process. Additionally, a normal photoelectron spectrum accompanied by its satellite structure, and Auger satellites arising from correlation or shake-up processes, appear in the spectra. Different contributions can be separated on the basis of a detailed comparison between theoretical calculations and experiment. Such a comparison was recently carried out for Xe,[2] and will be presented for Kr in this work. In addition, a careful theoretical study and comparison with experiment is also done for the normal $M_{4,5}NN$ transitions, which form a reference spectrum for the resonance Auger spectra.

Experimentally, only the $M_5N_{2,3}N_{2,3}$ resonance Auger spectrum of Kr taken at 91.2 eV photon energy has been studied until now.[1] Because of the relatively small 3*d* photoionization cross section, measurements of the Kr Auger spectra are much more difficult than those of Xe. In this paper we report, besides the $M_5N_{2,3}N_{2,3}$ resonance Auger spectrum, also the whole M_5NN resonance spectrum as well as the M_4NN resonance transitions. In this work we focus on those transitions which result after selective excitations of the 3*d* electrons, or ionization reasonably far from threshold. Thus the postcollision interaction (PCI) is left outside the scope of this work.

II. EXPERIMENTAL

The experimental measurements were made by using photons from the Canadian Synchrotron Radiation Facility at the Tantalus storage ring, and a Leybold-Heraus LHS-11 spectrometer mounted at the magic angle.[5] The electron intensities are thus independent of β and the po-

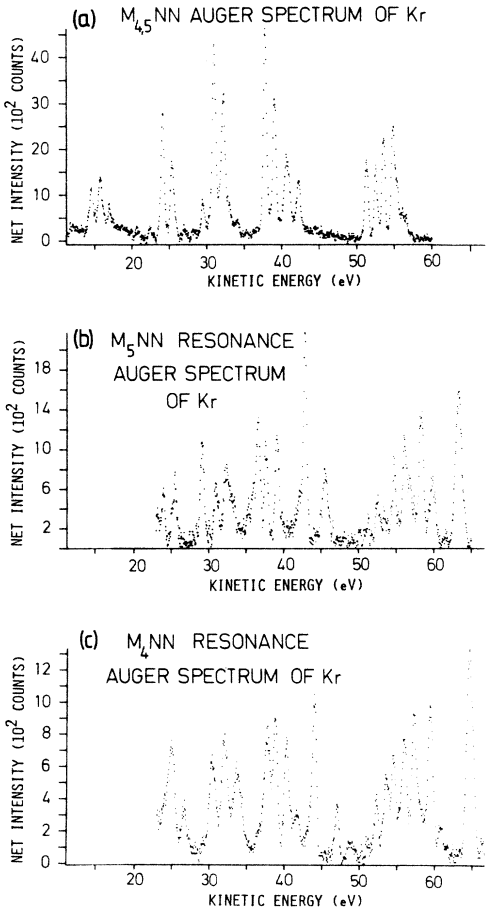

FIG. 1. Auger and resonace Auger spectra of Kr recorded using (a) 110 eV photon enrgy to ionize the 3*d* levels, (b) 91.2-eV photons to excite the $3d_{5/2}$ electrons to the 5*p* Rydberg state, and (c) 92.4-eV photons to excited the $3d_{3/2}$ electrons.

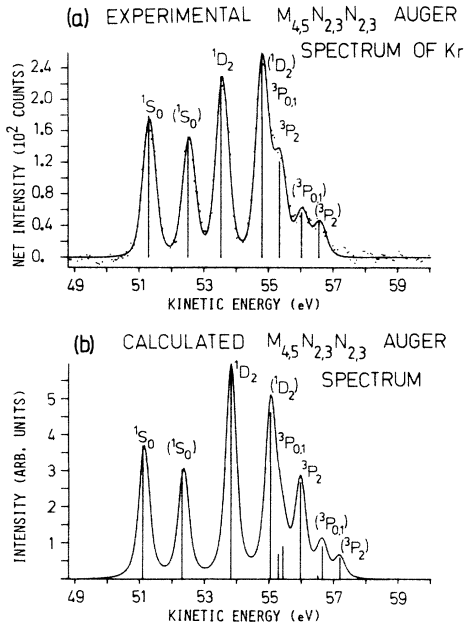

FIG. 2. Comparison between (a) experimental and (b) calculated $M_{4,5}N_{2,3}N_{2,3}$ Auger electron spectra. *LS* symbols in parentheses refer to the M_4 group and those without brackets to the M_5 group.

larization of the incident radiation. The analyzer is working in the constant-pass-energy mode with the result that the analyzer transmission function is independent of the initial kinetic energy. All spectra were recorded at a monochromator bandwidth of 2 Å, and an electron analyzer pass energy of 50 eV.

Figure 1(a) shows the entire normal $M_{4,5}NN$ Auger electron spectrum of Kr measured using 110 eV photon energy to ionize the $3d$ levels. Figures 1(b) and 1(c) show the resonance spectra after excitation of Kr to the $3d^9 4s^2 4p^6(^3D_{5/2})5p$ and $3d^9 4s^2 4p^6(^2D_{3/2})5p$ resonance states at 91.2- and 92.4-eV photon energies. Besides the $3d_{3/2} \rightarrow 5p$ excitation at 92.4 eV photon energy, the $3d_{5/2} \rightarrow 6p$ excitation is also possible.

Energy calibration was carried out with the aid of the $M_5N_1N_{2,3}(^1P_2)$ and $M_4N_{2,3}N_{2,3}(^1S_0)$ Auger lines of Kr with energies of 37.84 and 52.58 eV, respectively.[6] The experimental $M_{4,5}N_{2,3}N_{2,3}$ spectrum [Fig. 2(a)] was decomposed into the line components by a computer code CRUNCH.[7] The best fit was obtained with 0.47 eV full width at half maximum (FWHM) for the standard-line-shape Voigt functions. The same width and shape of the Voigt function was used to form the theoretical profiles.

III. DISCUSSION

A. $M_{4,5}NN$ Auger transitions

Normal $M_{4,5}NN$ Auger transitions shown in Fig. 1(a) consist of five line groups. Each group shows a doublet structure due to the spin-orbit splitting in the initial state of the Auger decay. The high-kinetic-energy structure (at 50–60 eV) is due to the $M_{4,5}N_{2,3}N_{2,3}$ transitions. The $M_{4,5}N_1N_{2,3}$ transitions on the low-kinetic-energy side (at 28–45 eV) split into the parent and satellite lines, which lie almost 10 eV from each other. The same kind of double structure can be seen in the case of the $M_{4,5}N_1N_1$ transitions on the lowest-kinetic-energy side of the spectrum (at 12–28 eV).

In our previous paper[6] the analysis of the fine structure was discussed in detail on the basis of the relativistic multiconfiguration calculations for the transition energies. In this paper we present a comparison with calculated profiles; thus also the theoretical intensities are given. Such a comparison is done for normal as well as resonance Auger transitions. The same kind of study was carried out very recently for the $N_{4,5}OO$ spectrum of Xe.[2]

Energies of the transitions are obtained in the self-consistent-field method as the difference of the energy levels of the initial and final states (the ΔSCF method). The calculations are carried out with the computer code MCDF of Grant *et al.*[8] The Coulomb interaction is used as the operator in the matrix element to calculate the transition probabilities within Fermi's golden rule. The open-shell structure is completely taken into account in the case of the resonance Auger transitions with a spectator electron. Radial integrals are obtained from the tables of McGuire.[9]

Figure 2 shows the experimental and calculated $M_{4,5}N_{2,3}N_{2,3}$ Auger profiles of Kr. The calculated profile was obtained with the single-configuration approach. Agreement with experiment is very good. Due to the overestimation in the calculated energy splitting, the $M_5N_{2,3}N_{2,3}(^3P_{0,1,2})$ lines overlap more with the $N_4N_{2,3}N_{2,3}(^1D_2)$ line in the experimental spectrum than in the calculated one. The experimental absolute energies are about 0.2 eV lower than the calculated ones. The intensity distribution between the $^1D_2$ and $^1S_0$ lines is fairly well reproduced by the single-configuration approach. Agreement is better than obtained recently for the $N_{4,5}O_{2,3}O_{2,3}$ transitions of Xe.[2]

Next we compare the calculated and experimental $M_{4,5}N_1N_{2,3}$ profiles. Figure 3 shows the experimental $M_{4,5}N_1N_{2,3}$ Auger spectrum of Kr [Fig. 3(c)] along with the calculated spectra [Figs. 3(a) and 3(b)]. Due to the decay of the $4s$ hole state by the $4s^1 \rightarrow 4s^2 4p^4 ns,nd$ process, the $3d^9 \rightarrow 4s^1 4p^5$ transitions split into parent and satellite structures. The lines due to the $4s^1 4p^5$ Auger strength [Fig. 3(a)] are considerably shifted and their intensity is redistributed between the parents and the satellites, which result from the $4s^1 4p^5 \rightleftarrows 4s^2 4p^3 ns,nd$ ($n = 4,5,\ldots,\epsilon$) decay and fluctuations.

We use the nomenclature main or parent and satellite lines, even if it is of purely notational value,[2] in order to make the comparison with analogous photoelectron studies easier. The appearance of the strong satellite structure in the $4s$ photoelectron and $M_{4,5}N_1N_{2,3}$ Auger spectrum of Kr can be analyzed either in terms of diagrammatic techniques considering an Auger or Coster-Kronig type of decay, or in terms of the configuration interaction considering the mixture between the configuration with a $4s$ hole and the configuration with two $4p$ holes and one excited electron. As in the previous paper,[2] the latter approach is employed to carry out the actual computations

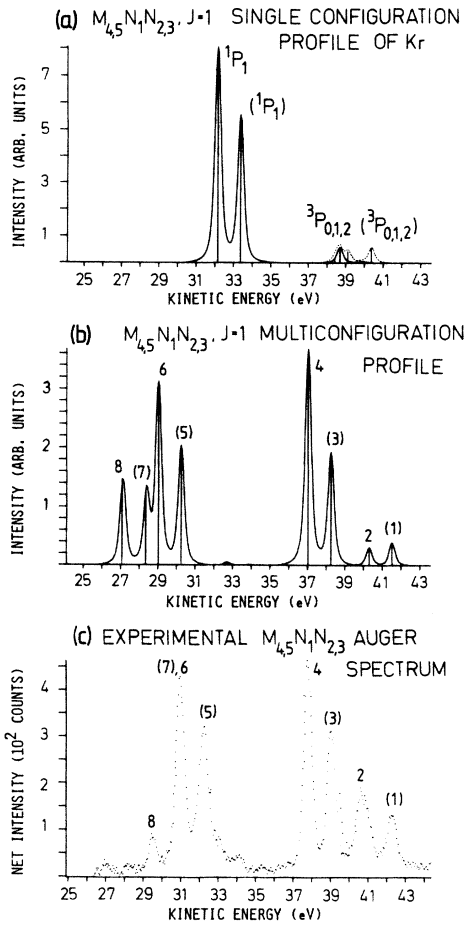

FIG. 3. Comparison between calculated (a) single-configuration and (b) multiconfiguration profiles with the experimental $M_{4,5}N_1N_{2,3}$ Auger spectrum (c). Numbered peaks are discussed in the text.

in this paper.

The single-particle picture is completely unable to give a good description for the transitions as expected. This is demonstrated when the single-particle theory [Fig. 3(a)] is compared with experiment [Fig. 3(c)]. By taking into account the correlation between the $4s^14p^5$ and $4s^24p^34d$ final-state configurations, the calculated profile of Fig. 3(b) results. This profile is in a much better agreement with experiment. A limited basis set was used and an optimal level calculation carried out with the MCDF code of Grant[8] to obtain the wave functions and mixing coefficients for the formation of the theoretical profile. The basis set contained, in addition to the relativistic $4s^14p^5$ configurations, only those relativistic configurations of the $4s^24p^34d$ type, which mix most strongly with the $4s^14p^5$ ones. (For example, the nonrelativistic $4s^14p^5$ configuration gives two relativistic ones, the $4s^14\bar{p}^5$ and the $4s^14p^5$, where $\bar{p}$ refers to $p_{1/2}$ and p to $p_{3/2}$.) This choice of the basis set was found to be a fairly good compromise to avoid time-consuming computations, which result if all the nd ($n=4,5,\ldots,\epsilon$) configurations are taken into account. By optimizing the lowest energy level with the strongest $4s^14p^5$ contribution, improper increase of the satellite intensity was eliminated. Mixing with the $4s^24p^3ns$ configurations was found to be of minor importance in our earlier work[2] and was thus neglected. Because of insufficient computer resources, it was not possible to carry out more extensive computations in this connection. As pointed out by Smid and Hansen[10] in the case of the photoelectron spectrum, a better description could be obtained by using a more extended basis set. Present computations, however, reproduce the experimental fairly well, although they slightly overestimate the shift between the main (1—4) and the satellite (5—8) structures.

Peaks 1 and 2 in the theoretical profile [Fig. 3(b)] are due to the transitions from the $3d_{3/2}$ and $3d_{5/2}$ initial hole states to the $4s^14p^5(^3P_1)$ final state. They correspond to the peaks 1 and 2 in the experimental spectrum. The $4s^14p^5(^3P_0$ and $^3P_2)$ lines fall into the same energy region with the $4s^14p^5(^3P_1)$ lines, and cause the increase of the intensity in the experiment. In the calculated profile [Fig. 3(b)] they have not been taken into account. The redistribution of the intensity of the $^1P_1$ lines between the parent lines 3 and (and 4) and the satellites 6 and 8 (and 5 and 7) is fairly well reproduced by the present computa-

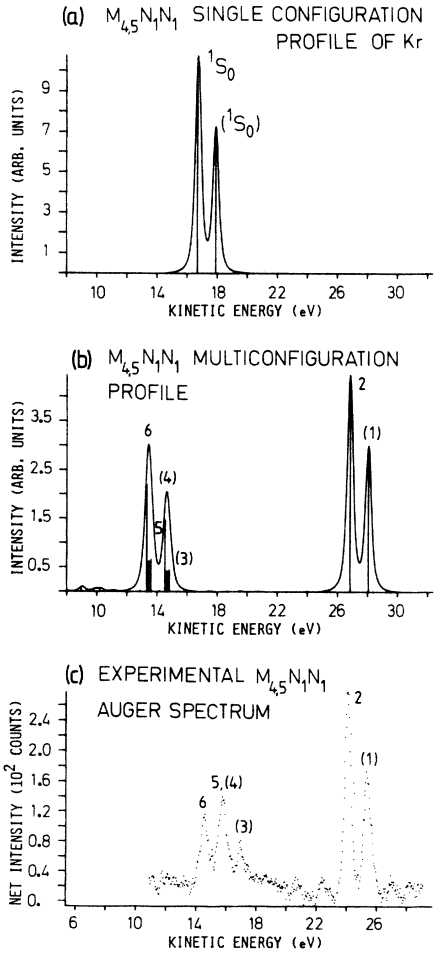

FIG. 4. Comparison between calculated (a) single-configuration and (b) multiconfiguration profiles with the experimental $M_{4,5}N_1N_1$ Auger spectrum (c).

tions. (Transitions from the $3d_{5/2}$ hole state are given without parentheses, and those from the $3d_{3/2}$ hole state with parentheses in the text as well as in the figures.) The intensity of peak 8 is clearly overestimated by theory. This is mainly due to the use of the limited basis set, and probably could be eliminated by using an extended basis set, which takes into account the excitations to the higher

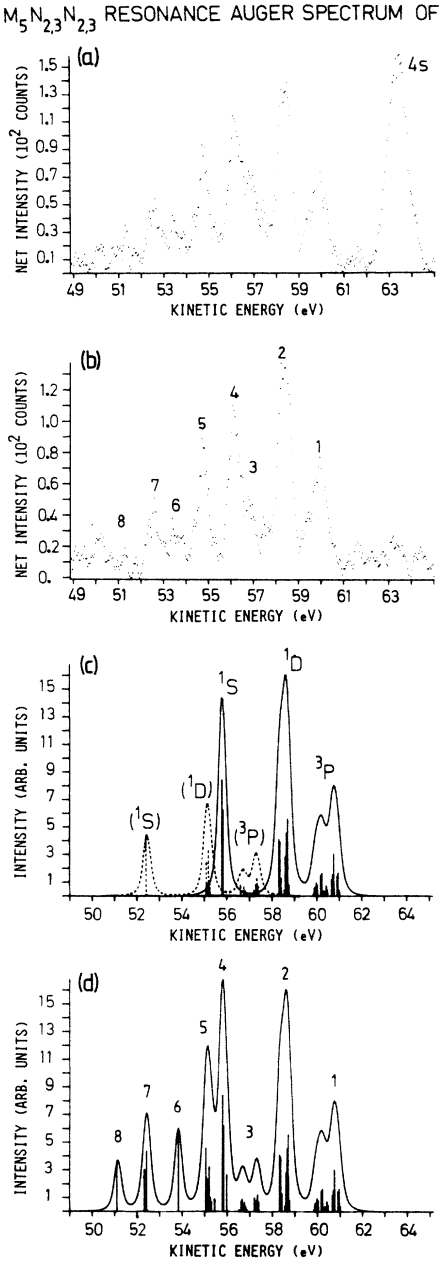

FIG. 5. (a) Experimental $M_5N_{2,3}N_{2,3}$ resonance Auger spectrum of Kr taken at 91.2±0.2 eV photon energy, and (b) after subtraction of the 4s photoelectron spectrum shown in Fig. 5. (c) Calculated $3d^9_{5/2}5p \rightarrow 4p^45p$ (solid line) and $3d^9_{5/2}5p \rightarrow 4p^46p$ (dashed line) profiles. Term symbols without parentheses refer to the parent $4p^4$ configuration of the $3d^9_{5/2}5p \rightarrow 4p^45p$ decay and with parentheses to those of the $3d^9_{5/2}5p \rightarrow 4p^46p$ decay. (d) Sum of profiles shown in (c) and in Fig. 2(b), obtained as discussed in the text.

Rydberg states as well as to the continuum. The shoulder on the high energy side of peak 5 [Fig. 3(c)] is due to the satellites which result from the final-state correlation between the $4s^24p^34d$ configuration and the $4s^14p^5(^1P_1)$ and $4s^14p^5(^3P_1)$ states. The limited basis set seems to be unable to reproduce correctly their intensity and energy.

Figure 4 shows the experimental $M_{4,5}N_1N_1$ Auger spectrum of Kr [Fig. 4(c)] along with the theoretical calculations. A single-configuration profile, corresponding to the $3d^9_{5/2,3/2} \rightarrow 4s^0(^1S_0)$ decay, shows a simple doublet structure [Fig. 4(a)]. In experiment [Fig. 4(c)], the main lines are considerably shifted and an extra structure appears at lower energy by about 10 eV. Multiconfiguration calculations, which take into account the correlation between the $4s^04p^6$, $4s^14p^44d^1$, and $4s^24p^24d^2$ configurations, give a profile depicted in Fig. 4(b). The computations were carried out by optimizing the wave functions and the mixing coefficients for the lowest energy level.

The multiconfiguration profile shows the main lines 1 and 2, corresponding to the transitions from the $3d_{3/2}$ and $3d_{5/2}$ initial hole states to the final state which has the strongest $4s^04p^6$ contribution, in fairly good agreement with experiment. The satellites are generated from three line components in both the M_5 and M_4 groups, but the components lie very close to each other, thus forming one peak in both groups. Experiment [Fig. 4(c)], however, shows a clear doublet structure where the low-energy component (4) of the M_4 group overlaps with the high-energy component 5 of the M_5 group. Furthermore, the energy separation between the main lines (1 and 2) and the satellites (3—6) is considerably overestimated by theory. Calculations predict extra satellites with noticeable intensity at 3.7 and 4.5 eV kinetic energies, but due to the rapid increase of the background at very low kinetic energies, it has not been possible to confirm this experimentally.

The satellite intensity relative to the parent intensity strongly increases in going from the 4s photoelectron spectrum to the Auger electron spectra. In the former case (Fig. 5) the satellite-to-parent ratio of 0.63 is obtained experimentally, whereas the values of 0.84 and 0.90 are derived by taking the ratios of the averaged intensities of satellite and parent structures of the $M_{4,5}N_1N_{2,3}$ [Fig. 3(c)] and $M_{4,5}N_1N_1$ [Fig. 4(c)] spectra. This indicates that the correlation effects are very sensitive to the degree of the ionization and the states of the other electrons.

B. Resonance Auger transitions

The $M_{4,5}N_{2,3}N_{2,3}$ resonance Auger spectra were presented by Eberhardt *et al.*[1] some time ago and a general discussion of the structure was given at the same time. In this work we carry out a thorough comparison between the experimental and calculated profiles. In this way it is possible to analyze in detail the different contributions which form the experimental profiles shown in Figs. 6 and 7.

Figures 5 and 6 present the resonance spectra, excited at 91.2- and 92.4-eV photon energies [Figs. 5(a) and 6(a)], compared to the theoretical calculations. In order to obtain pure resonance Auger spectra which are free from the contributions of the satellite structure accompanying the

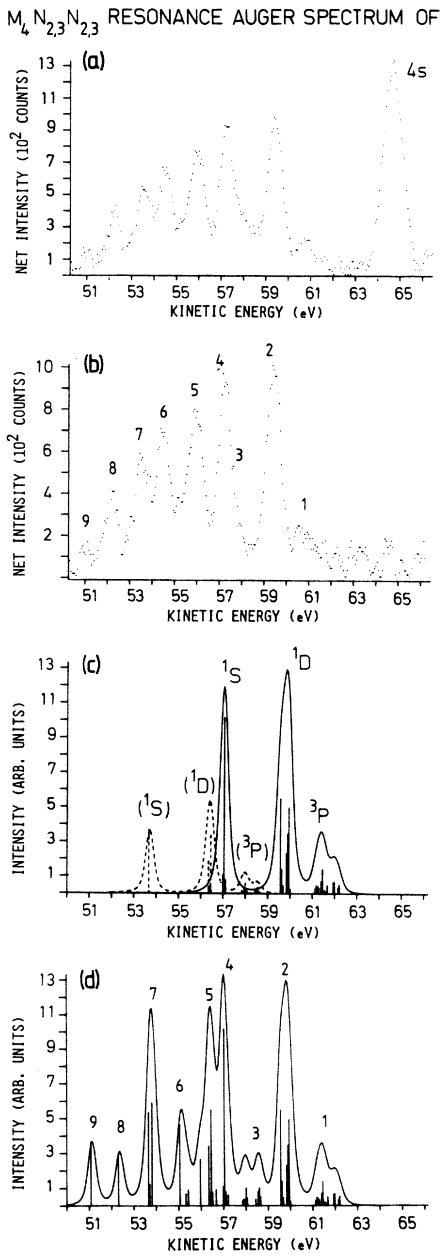

FIG. 6. $M_4N_{2,3}N_{2,3}$ resonance Auger spectrum at 92.4 eV photon energy. See caption of Fig. 5 for detailed description. Sum profile (d) contains the $3d^9_{5/2}6p \rightarrow 4p^6 6p$ spectrum, too.

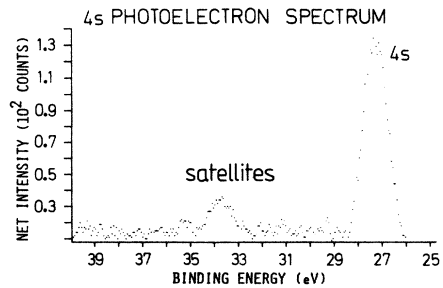

FIG. 7. 4s photoelectron spectrum taken at 100 eV photon energy. This spectrum has been subtracted from the M_5 and M_4 resonance Auger spectra (Figs. 6 and 7).

4s photoelectron line, the 4s photoelectron spectrum (Fig. 7) was first subtracted. Figures 5(b) and 6(b) show the spectra after this subtraction. The interference effects between the resonance Auger spectra with the excited electron as the spectator and the satellite spectra may play a prominent role, because the final state of the spectator transition is the same as the final state of the shake-up satellite, where a $5p \rightarrow 6p$ shakeup accompanies the 4s photoionization. In Xe the interference effects were found to be negligible.[2] The subtraction of the 4s photoelectron line neglects, in addition to the interference effects, also the contribution due to the autoionization process, where the excited electron takes part in the transition. Good agreement between calculated and experimental profiles clearly supports the assumption that autoionization involving the excited electron, and interference effects, are of minor importance in Kr, as was also found for Xe.[2] The excited state thus dominantly decays by the resonance Auger process where the excited electron remains as the spectator.

After excitation of Kr to the $3d^94s^24p^6(^2D_{5/2})5p$ resonance state at 91.2 eV photon energy, the transitions of the $3d^9_{5/2}5p \rightarrow 4p^45p$ type are expected. The solid curve in

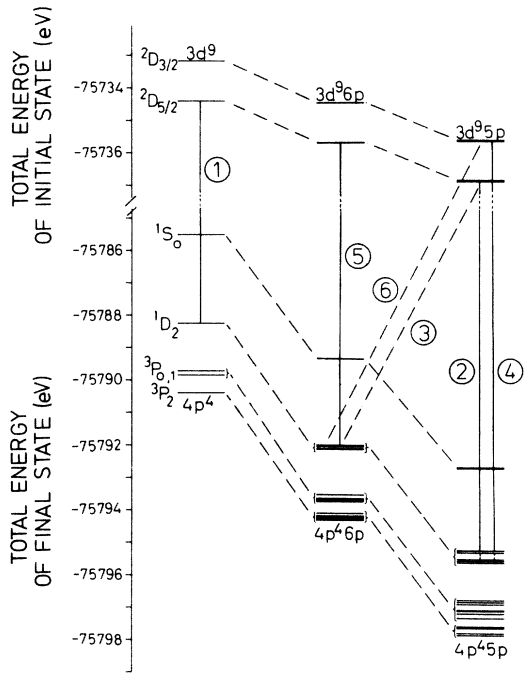

FIG. 8. Calculated energy levels $3d^9(^2D_{5/2})$, $3d^9(^2D_{3/2})$, $3d^9(^2D_{5/2})6p$, $3d^9(^2D_{3/2})6p$, $3d^9(^2D_{5/2})5p$, and $3d^9(^2D_{3/2})5p$ of the initial states, and $4p^4(^{2S+1}L_J)$, $4p^4(^{2S+1}L)6p$, and $4p^4(^{2S+1}L)5p$ of the final states of the transitions. Computations are carried out with the Dirac-Fock code of Grant (Ref. 8). Vertical lines display the following transitions. 1: $3d^9(^2D_{5/2}) \rightarrow 4p^4(^1D_2)$, which gives the most intense peak $^1D_2$ in Fig. 2(b). 2: $3d^9(^2D_{5/2})5p \rightarrow 4p^4(^1D)5p$ resulting in peak ^1D of Fig. 5(c). 3: $3d^9(^2D_{5/2})5p \rightarrow 4p^4(^1D)6p$ resulting in peak (^1D) of dashed line in Fig. 5(c). 4: $3d^9(^2D_{3/2})5p \rightarrow 4p^4(^1D)5p$ giving the most intense peak ^1D in Fig. 6(c). 5: $3d^9(^2D_{5/2})6p \rightarrow 4p^4(^1D)6p$, which contributes to peak 5 of Fig. 6(c). 6: $3d^9(^2D_{3/2})5p \rightarrow 4p^4(^1D)6p$ shown by dashed line (^1D) in Fig. 6(c), which also contributes to peak 5 of Fig. 6(c).

Fig. 5(c) represents the profile calculated for the $3d^9_{5/2} \rightarrow 4p^4$ decay with a $5p$ spectator electron. Extra splitting, due to the coupling of the $5p$ electron with the electrons participating in the transition, is completely taken into account. Term symbols given in Fig. 5(c) refer to the parent $4p^4$ configuration. The vertical lines show the daughters caused by the coupling of the spectator electron, and the curve represents their sum profile. It is broadened due to the overlap of several close-lying daughter lines around each peak. This broadening, due to the open-shell structure, is also apparent in the experiment in going from the normal [Fig. 2(a)] to resonance [Fig. 5(b)] Auger spectrum.

In more detail the differences between the normal and spectator Auger spectra are illustrated in Fig. 8, which presents the energy levels of the initial and final states obtained from the MCDF calculations, for each transition. Vertical line 1 on the left side describes the $3d^9(^2D_{5/2}) \rightarrow 4p^4(^1D_2)$ transition which takes place after ionization of the $3d$ level. On the right side we see the energy levels of the $3d^9np$ and $4p^4np$ ($n=5,6$) configurations. Splitting of the $4p^4(^1D_2)$ level to the daughters in the presence of an np electron is visible. Vertical line 2 on the right side illustrates the $3d^9(^2D_{5/2})5p \rightarrow 4p^4(^1D)5p$ transition.

By comparing the solid curve in Fig. 5(c) representing the $3d^9_{5/2}5p \rightarrow 4p^45p$ decay with experiment, the main peaks can be identified. Peak 1 in Fig. 5(b) corresponds to the transitions from the $3d^9(^2D_{5/2})5p$ resonance state to the $4p^4(^3P)5p$, peak 2 to the $4p^4(^1D)5p$, and peak 4 to the $4p^4(^1S)5p$ final state. In addition to this, strong structure appears on the high-energy side of peak 4. Peak 5 cannot be identified to correspond to the $3d^95p \rightarrow 4p^45p$ transitions, either. Dashed lines in Fig. 5(c) show the transitions from the $3d^9(^2D_{5/2})5p$ initial state to the $4p^46p$ final states. By comparing this profile with experiment, we assign peaks 5 and 3 to transitions to the $4p^4(^1D)6p$ and $4p^4(^3P)6p$ final states. The $3d^9(^2D_{5/2})5p \rightarrow 4p^4(^1S)6p$ decay takes place around peak 7. [The $3d^9(^2D_{5/2})5p \rightarrow 4p^4(^1D)6p$ transitions are described by the dashed line 3 in Fig. 8, too.] The transitions, where the $5p \rightarrow 6p$ shake-up takes place during the Auger decay, thus occur with a remarkable intensity. This is consistent with the finding for Xe, where the $4d^96p \rightarrow 5p^46p$ transitions are accompanied by the $4d^96p \rightarrow 5p^47p$ transitions.

Peaks 3 and 5 fit energetically also to the $3d^9_{5/2}6p \rightarrow 4p^4(^1D)6p$ and $3d^9_{5/2}6p \rightarrow 4p^2(^1S)6p$ transitions, which could occur due to the direct $3d_{5/2} \rightarrow 6p$ excitation. With our photon energies, this excitation should not play a strong role, even at the rather large bandwidth (0.6 eV) used in the measurements and the uncertainty of our photon energy of 0.2 eV. The intensity ratio of peaks 3 and 5 in the experimental spectrum does not correspond to the calculated ^1D-to-^1S ratio either. Thus, peaks 3 and 5 may mainly be caused by the shake-up transitions $3d^9_{5/2}5p \rightarrow 4p^46p$. The $3d^1_{5/2}6p \rightarrow 4p^46p$ transitions are expected to cause only a small contribution to the intensity of peaks 3 and 5.

Extra structure at the low-energy side of the spectrum of Fig. 5(b) may be due to the $M_{4,5}N_{2,3}N_{2,3}$ transitions originating from the ionization by second- and higher-order diffracted light and by scattered light in the photon beam. Calculated transitions $M_{4,5}N_{2,3}N_{2,3}(^1S_0)$ fit energetically with the structures 7 and 8 in Fig. 6(d). The $M_{4,5}N_{2,3}N_{2,3}(^1D_2)$ lines contribute to peaks 5 and 6 in Fig. 5(d). The $M_{4,5}N_{2,3}N_{2,3}(^3P)$ lines lie under peak 4. Due to the poor statistics caused by low counting rates, detailed interpretation of the structure in the 50—54-eV energy region is very difficult.

In Fig. 5(d) we show a sum spectrum formed by using relative intensities of 100, 30, and 25 for the $3d^9_{5/2}5p \rightarrow 4p^45p$, $3d^9_{5/2}5p \rightarrow 4p^46p$, and $3d^9 \rightarrow 4p^4$ transitions, respectively. A numbering analogous to that of Fig. 5(b) is given for the main peaks of the calculated sum profile (solid curve). Agreement with experiment is fairly good. The ^1D-^1S energy splitting is slightly overestimated by theory. This results in the stronger overlap of peaks 4 and 5 in experiment than in theory.

By taking a look at Fig. 8, we find that the spectator transitions $3d^9np \rightarrow 4p^4np$ give higher kinetic energies than the $3d^9 \rightarrow 4p^4$ transitions. Energies are obtained by the ΔSCF method, and vertical lines 1, 2, and 5 thus display the energies of the normal and spectator ($np=5p$ or $6p$) transitions. The spectator spectra thus shift to higher energies from the normal spectra. Compared to the measured normal Auger spectrum [Fig. 2(a)], the ^1D line is found to shift by 4.8 eV in going to the resonance transition with a $5p$ spectator electron. Theory reproduces the shift excellently, also giving a value of 4.8 eV. Peak 5 is shifted by 1.2 eV from the $^1D_2$ line of the normal spectrum in experiment. The shift is consistent with the calculated value of 1.4 eV for the $3d^1_{5/2}5p \rightarrow 4p^4(^1D)6p$ transition.

For the $M_4N_{2,3}N_{2,3}$ resonance Auger transitions (Fig. 6) the situation is much the same as discussed above for the $M_5N_{2,3}N_{2,3}$ resonance Auger spectrum. At 92.4 eV photon energy, the $3d_{3/2}$ electron is excited to a $5p$ orbital. A strong contribution in the Auger electron spectrum is due to the transitions with a $5p$ spectator electron. This can be seen by comparing experiment [Fig. 6(b)] with the calculated profiles of Fig. 6(c). Besides, a considerable amount of the shake-up transitions $3d^9_{3/2}5p \rightarrow 4p^46p$ and the normal Auger transition exist in the spectrum. Furthermore, the $3d^9_{5/2}6p \rightarrow 4p^46p$ resonance Auger spectrum overlaps with the low-energy part of the M_4 resonance spectrum. This is because the photon energy of 92.4 eV used for the $3d_{3/2} \rightarrow 5p$ excitation is also able to excite the $3d_{5/2}$ electron to an empty $6p$ level due to a very small energy deviation in the excitation energies (92.4 and 92.5 eV). This is also visible in Fig. 8, where the $3d^9(^2D_{3/2})5p$ and $3d^1(^2D_{5/2})6p$ energy levels match well energetically. Solid lines 4 and 5 in Fig. 8 illustrate the $3d^9(^2D_{3/2})5p \rightarrow 4p^4(^1D)5p$ and $3d^9(^2D_{5/2})6p \rightarrow 4p^4(^1D)6p$ decays, respectively. Dashed line 6 (Fig. 8) displays the shake-up transition $3d(^2D_{3/2})5p \rightarrow 4p^4(^1D)6p$.

Figure 6(d) shows a sum profile, where relative intensities of 100, 30, 25, and 30 have been used for the $3d^9_{3/2} \rightarrow 5p \rightarrow 4p^45p$, $3d^9_{3/2}5p \rightarrow 4p^46p$, $3d^9 \rightarrow 4p^4$, and $3d^9_{5/2}6p \rightarrow 4p^46p$ transitions, respectively. The peaks labeled by 1—9 match with the corresponding experimental peaks of Fig. 6(b). Peak 1 is due to the $3d^9_{3/2}5p \rightarrow 4p^4(^3P)5p$ transitions and peak 2 to the $3d^9_{3/2}5p$

$\rightarrow 4p^4(^1D)5p$ transitions. Peak 4 corresponds to the $3d^9_{3/2}5p \rightarrow 4p^4(^1S)5p$ decay. The high-energy shoulder of it shown in Fig. 6(b) can be assigned to the $3d^9_{3/2}5p \rightarrow 4p^4(^3P)6p$ transitions. The $3d^9_{3/2}5p \rightarrow 4p^4(^1D)6p$ and the $3d^9_{5/2}6p \rightarrow 4p^4(^1D)6p$ transitions mainly form peak 5. Peak 6 arises from the normal $3d^9_{3/2} \rightarrow 4p^4(^1D_2)$ decay. Structure 7 is due to the $3d^9_{3/2}5p \rightarrow 4p^4(^1S)6p$, the $3d^9_{5/2}6p \rightarrow 4p^4(^1S)6p$, and the normal $3d^9_{5/2} \rightarrow 4p^4(^1D_2)$ transitions. Experimentally the ^1S lines are shifted to higher energies, but in the theoretical estimate they overlap with the ^1D line thus overestimating the intensity of the peak 7. Peaks 8 and 9 result from the transitions from the $3d_{3/2}$ and $3d_{5/2}$ initial hole states to the $4p^4(^1S_0)$ final state. In addition, the $M_{4,5}N_{2,3}N_{2,3}(^3P)$ lines, with and without a spectator electron, overlap with the other lines. Because they have a very low intensity, their contribution in the formation of the peaks is of minor importance.

The energy shift of the $M_5N_{2,3}N_{2,3}(^1D)$ line between the normal and the resonance Auger spectrum with a $5p$ spectator electron was found to be 4.6 eV experimentally. The calculated value of 4.8 eV agrees very well. Energy shifts, caused by a spectator, are thus fairly well reproduced by theory. A value of 1.0 eV was obtained for the normal to shake-up ($5p \rightarrow 6p$) shift from the experiment, whereas the estimation from the calculations is 1.4 eV.

Next we consider the $M_{4,5}N_1N_{2,3}$ resonance Auger spectra, which are depicted in Figs. 9 and 10. The experimental spectra [Figs. 9(a) and 10(a)] show a rich fine structure. The main and correlation satellite lines appear in the spectra as multiplied, because the spectator, shake-up, and normal transitions all contribute as in the $MN_{2,3}N_{2,3}$ group. Due to the convergence problems we were not able to carry out calculations for these spectator transitions. Therefore we have used an approximate approach to produce a calculated sum profile: Peaks 2, 4, 6, and 8 of Fig. 3(b), which result from the $M_5N_1N_{2,3}$ decay, were shifted by 4.8 eV corresponding to the resonance Auger profile with a $5p$ spectator electron [peaks 1, 2, 5, and 5′ in Fig. 9(b)], and by 1.4 eV corresponding to the Auger decay accompanied by the $5p \rightarrow 6p$ shakeup. (The shifts were calculated above for the $MN_{2,3}N_{2,3}$ group.) Peaks (1), (3), (5), and (7) were shifted analogously in the case of the $M_4N_1N_{2,3}$ group [Fig. 10(b)]. These profiles and the $M_{4,5}N_1N_{2,3}$ spectrum were then summed using the same portions for different contributions as in the case of the $MN_{2,3}N_{2,3}$ resonance shown in Figs. 5(d) and 6(d). The sum profiles are depicted in Figs. 9(c) and 10(c).

The energy splitting between the main and satellite lines was overestimated by theory in the $M_{4,5}N_1N_{2,3}$ group (Fig. 3). The main (1,2) and satellite (5,5′) lines in Figs. 9(b) and 10(b) thus lie too far from each other. The intensity of satellites, especially that of line 5′, is also overestimated. Therefore, the structure of the sum profiles [Figs. 9(c) and 10(c)] is not expected to perfectly correspond to the observed resonance profiles [Figs. 9(a) and 10(a)]. However, the sum profiles are useful, together with the above-mentioned findings for the $MN_{2,3}N_{2,3}$ resonance spectra (Figs. 5 and 6) and for the $M_{4,5}N_1N_{2,3}$ spectrum (Fig. 3), in the interpretation of the observed structures of Figs. 9(a) and 10(a). Peaks 1 and 2 correspond to the transitions from the $3d^2_{5/2}5p$ [Fig. 9(a)] and $3d^9_{3/2}5p$ [Fig. 10(a)] resonance states to the $4s^14p^5(^3P)5p$ and $4s^14p^5(^1P)5p$ final states, respectively. Peak 5 may be assigned to the correlation satellite accompanying peak 2, which is due to the mixture of the $4s^14p^5(^1P)5p$ and $4s^24p^34d(^1P)5p$ states. The mixing also causes the shift of peak 2 to higher kinetic energies from its single-configuration prediction. An alternative nomenclature for the appearance of the satellite structure and the energy shift could be the resonance double Auger process $3d^95p \rightarrow 4s^14p^55p \rightleftarrows 4s^24p^34d\,5p$, where the second Auger electron is not ionized, but excited to a Rydberg state.

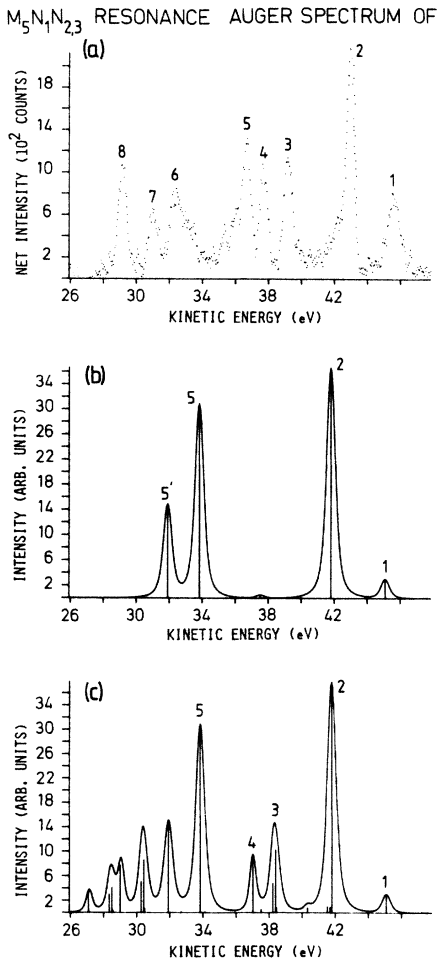

FIG. 9. (a) Experimental $M_5N_1N_{2,3}$ resonance Auger spectrum of Kr recorded using 91.2-eV photons. (b) Profile for the $3d^9_{5/2}5p \rightarrow 4s^14p^55p \rightleftarrows 4s^24p^34d\,5p$ decay, obtained by shifting peaks 2, 4, 6, and 8 of Fig. 3 by 4.8 eV, and (c) sum spectrum obtained as discussed in the text.

Peak 3 in Figs. 9(a) and 10(a) is due to the $3d^95p \rightarrow 4s^14p^5(^1P)6p$ transition, and peak 6 to its correlation satellite resulting from the $4s^14p^56p \rightleftarrows 4s^24p^34d\,6p$ decay and fluctuations. The $M_{4,5}N_1N_{2,3}$ transitions arising from the second-order and diffracted light contribute to peaks 3 and 4 in the M_5 [Fig. 9(a), see also Fig. 9(c)] and to peaks 4 and 5 in the M_4 [Fig. 10(a), peaks 4 and 5″ in Fig. 10(c)] resonance spectrum. Their satellites, furthermore, contribute to peaks 6 and 7 in the M_5 [Fig. 9(a)],

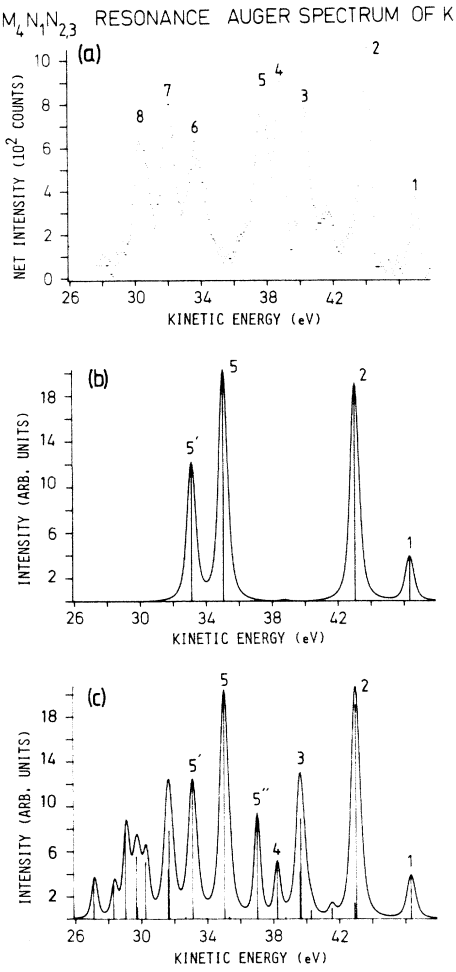

FIG. 10. (a) Experimental $M_4N_1N_{2,3}$ resonance spectrum of Kr obtained at 92.4 eV photon energy. (b) Profile for the $3d_{3/2}^9 5p \rightarrow 4s^1 4p^5 5p \rightleftarrows 4s^2 4p^3 4d\,5p$ decay, obtained by shifting peaks (1), (3), (5), and (7) of Fig. 3 by 4.8 eV, and (c) sum spectrum.

and to peaks 7 and 8 in the M_4 [Fig. 10(a)] group. The overestimation of the intensity of peaks 5 and 5′ and their energy difference from peak 2 [Figs. 9(b) and 10(b)] causes the main discrepancy between experimental [Figs. 9(a) and 10(a)] and calculated [Figs. 9(c) and 10(c)] sum profiles. Peaks 5″ and 5 in Fig. 10(c) overlap in experiment [Fig. 10(a)] at peak 5, peak 5′ of Fig. 10(c) forming the low-energy shoulder of peak 5 in Fig. 10(a).

Peak 8 in Figs. 9(a) and 10(a) mainly arises from the $3d^9 5p \rightarrow 4s^0(^1S)5p$ transitions. Due to the increase of the background at low kinetic energies, it was not possible to observe the correlation satellite structure of the MM_1N_1 group in the resonance spectra. The outermost structure observed around 25 eV mainly arises from the $M_{4,5}N_1N_{2,3}(^1S_0)$ transitions after ionization by second-order light. High background, especially in Fig. 10(a), makes their intensity uncertain.

The $MN_1N_{2,3}(^1P_1)$ line is found to shift by 5.0 and 5.1 eV in the M_4 and M_5 spectra, in going from the ionization to the excitation of the $3d$ electron to the $5p$ orbital. For the $MN_1N_1(^1S_0)$ line the shifts of 5.0 eV were observed both in the M_4 and in the M_5 group. The shift of 4.8 eV from the $MN_{2,3}N_{2,3}$ spectrum does not agree with this finding. The differences in the energy shifts demonstrate the importance of the electron correlation. The correlation is present in the $MN_1N_{2,3}$ and MN_1N_1, but absent in the $MN_{2,3}N_{2,3}$ energy-shift values between the normal and resonance Auger spectra.

So far we have studied the decay of the $3d^9 5p$ resonance state, which results in an emission of one Auger electron. A highly excited final state of the process, with a spectator electron in the presence of two inner holes, may further Auger decay. The emission of the second Auger electron may now result, with the spectator electron now participating in the process. This true double Auger decay leaves the atom in a doubly ionized state. Relative to the spectator Auger, the double Auger structures lie about 6 eV lower in energy, according to the single-configuration Dirac-Fock predictions. Low-kinetic-energy sides of the main peak groups studied above may thus be further complicated due to actual double Auger structures. According to the foregoing analysis, the spectator and shake-up transitions form, however, the main peaks of the resonance spectra.

IV. CONCLUSIONS

The high-resolution $M_{4,5}NN$ normal and resonantly excited Auger spectra of Kr have been investigated by carrying out a detailed comparison between calculations and measurements taken by synchrotron radiation. At 91.2- and 92.4-eV photon energies, excited states $3d(^2D_{5/2})5p$ and $3d(^2D_{3/2})5p$ predominantly decay by the resonance Auger processes with the excited electron remaining as the spectator. Shakeup of the excited electron also takes place during the Auger decay. The $4s^1 4p^5 np \rightleftarrows 4s^2 4p^3 4dnp$ ($n = 5, \epsilon$) fluctuations cause strong energy shifts and redistributions of the intensity in the normal and resonance $M_{4,5}N_1N_{2,3}$ spectra. The same effect is also observed for the normal $M_{4,5}N_1N_1$ transitions. Single-configuration calculations fail to reproduce the correlation satellite structure, but our limited-basis-set multiconfiguration calculations lead to semiquantitative agreement with experiment. Even more extended basis sets are now needed in the computations. Due to insufficient computer resources their use was not possible in this work. The actual double Auger structure, which is not, howver, distinguishable from the background, may accompany the resonance Auger structure on their low-kinetic-energy side.

ACKNOWLEDGMENTS

We would like to acknowledge financial support from the National Research Council of Canada (NRC), the Natural Sciences and Engineering Research Council of Canada (NSERC), the University of Western Ontario, and the Finnish Academy of Science. We would also like to acknowledge the assistance of B. W. Yates and L. L. Coatsworth, and the helpful advice and assistance of the staff at the Synchrotron Radiation Center (Stoughton).

[1]W. Eberhardt, G. Kalkoffen, and C. Kunz, Phys. Rev. Lett. **41**, 156 (1978).

[2]H. Aksela, S. Aksela, G. M. Bancroft, K. H. Tan, and H. Pulkkinen, preceding paper, Phys. Rev. A **33**, 3867 (1986).

[3]S. Southworth, V. Becker, C. M. Truesdale, P. H. Kobrin, D. W. Lindle, S. Owaki, and D. A. Shirley, Phys. Rev. A **28**, 261 (1983).

[4]V. Schmidt, S. Krummacher, F. Wuilleumier, and P. Dhez, Phys. Rev. A **24**, 1803 (1981).

[5]B. W. Yates, K. H. Tan, L. L. Coatsworth, and G. M. Bancroft, Phys. Rev. A **31**, 1529 (1985).

[6]H. Aksela, S. Aksela, and H. Pulkkinen, Phys. Rev. A **30**, 2456 (1984).

[7]C. D. Akers, C. Pathe, J. J. Barton, F. J. Grunthaner, P. J. Grunthaner, J. D. Klein, B. F. Lewis, J. M. Rayfield, R. Ritchey, R. P. Vasquez, and J. A. Wurzbach, CRUNCH user's manual (California Institute of Technology, Pasadena, California, 1982).

[8]I. P. Grant, B. J. McKenzie, P. H. Norrington, D. F. Mayers, and N. C. Pyper, Comput. Phys. Commun. **21**, 207 (1980); **21**, 233 (1980).

[9]E. J. McGuire, Sandia Research Laboratory Research Report No. SC-RR-71-0835 (unpublished).

[10]H. Smid and J. E. Hansen, J. Phys. B **16**, 3339 (1983).